Hindawi
Advances in Materials Science and Engineering
Volume 2019, Article ID 9358740, 12 pages
https://doi.org/10.1155/2019/9358740

Research Article

Theoretical Analysis of the Optical Response of Silicon/Silica/Gold Multishell Nanoparticles in Biological Tissue

Wajdi Chaabani,[1,2] Abdallah Chehaidar,[1] Julien Proust,[2] and Jérôme Plain[2]

[1]*Laboratoire de Physique-Mathématiques et Applications, Université de Sfax, Faculté des Sciences de Sfax, B.P. 1171, 3000 Sfax, Tunisia*
[2]*Laboratoire de Nanotechnologie et d'Instrument Optique, Université de Technologie de Troyes, 12 rue Marie Curie, CS 42060, 10004 Troyes Cedex, France*

Correspondence should be addressed to Abdallah Chehaidar; abdallah.chehaidar@fss.rnu.tn

Received 27 November 2018; Accepted 6 January 2019; Published 3 February 2019

Academic Editor: Nezih Pala

The scattering and absorption efficiencies of light by a single silicon/silica/gold spherical multishell in biological tissues are analyzed theoretically in the framework of Lorenz–Mie theory and finite-difference time-domain formalism. We first revised the ideal case of a concentric silicon/gold nanoshell, analyzed the effect of growing a silica layer of uniform thickness around the silicon core, and then examined the effect of an offset of the gold shell with respect to the centre of the silicon/silica nanoshell. Our simulation showed that the silicon/gold nanoshell in the biological tissue supports significant absorption and scattering resonances in the biological spectral window. On the contrary, the growth of a silica layer on the silicon core surface leads to a blueshift of these resonances accompanied by a slight increase of their magnitudes. The offset of the gold shell with respect to the silicon/silica core results in a redshift of the absorption and scattering resonances supported by the concentric silicon/silica/gold multishell within the biological window, accompanied by a decrease in their amplitudes. On the contrary, the gold shell offset gives rise to a more prominent electric field enhancement at the silicon/silica/gold multishell-biological tissue interface. Our simulation thus shows that silicon/silica/gold multishell nanoparticles are potential candidates in bioimaging and photothermal therapy applications.

1. Introduction

In the last decade, metallic nanoparticles have known growing interest due to their unique electronic and optical properties that are dominated by the localized surface plasmon resonance (LSPR) [1]. A localized surface plasmon is a collective spatial oscillation of the conduction electrons in a metal nanoparticle. The interaction of LSPRs with incident light can either lead to an efficient scattering of light and/or absorption of light resulting in the metal heating. Hybrid core/shell nanoparticles with a dielectric core and a metallic shell have also aroused a particular interest; this interest is due to the fact that such the heterostructure provides additional degrees of freedom such as the material type and the relative core and shell sizes to tailor their optical response for specific applications. In particular, gold nanoshells have attracted significant attention for its application in biotechnology and biomedicine [2–11] because of its good biocompatibility and high chemical stability in addition to its tunable optical properties.

The occurrence of morphology-dependent LSPRs in metallic nanostructures has stimulated numerous simulation studies [12–27]. The simulation of interaction of light with metallic nanostructures is an important part of the scientific progress in the plasmonic field. In the one hand, the simulation technique is used in order to validate experimental measurements; on the other hand, it plays an important role in designing new nanostructures with specific properties. In the latter context, it fits our recent work [26] in which we have simulated the optical response of a single

silicon/gold core/shell concentric nanosphere in air. We have shown that this nanoshell model supports absorption resonances of light in the spectral range 600–1200 nm where the pure gold nanoparticle and SiO_2/Au nanoshell never absorb. This property is very interesting if one considers this kind of nanoshell in bioimaging and photothermal therapy applications.

In the present work, we proceed with the same model of nanostructure. But this time, we will discuss a deviation from an ideal structure, which is likely to be encountered in the growth phase. We thus envisage the growth of a thin silica layer just on the surface of the silicon core, on the one hand, and a break in the centrosymmetry caused by an offset between the centre of the SiO_2/Au core and that of the gold shell, on the other hand. A particular attention is devoted to the influence of silica shell thickness and the core offset on the scattering and absorption efficiencies of such Si/SiO_2/Au nanostructure embedded in a biological tissue.

2. Theoretical Approach

The problem consists of a single spherical particle of radius a embedded in a homogeneous nonabsorbing medium and illuminated by an electromagnetic plane wave propagating in the z direction, as illustrated schematically in Figure 1. The particle is a heterostructure composed of a silicon core cut in the form of a sphere of radius c coated with a concentric thin shell of silica of external radius b and a gold shell of external radius a. The offset between the centres of the Si/SiO_2 core/shell and the gold shell is designated as δ.

The interaction of the incident light with the nanoparticle is governed by Maxwell's equations. The resolution of these spatiotemporal partial differential equations, imposing boundary conditions at the Si-SiO_2, SiO_2-Au and Au-surrounding medium interfaces, allows determining the electromagnetic field $(\vec{E}, \vec{H})$ at any point inside and outside the particle.

The ability of a nanoparticle to scatter and to absorb incident light can be expressed by the scattering cross section C_{sca} and the absorption cross section C_{abs}. They represent the rate at which the incident radiation is scattered and absorbed by the particle, respectively; they are defined by the following equation:

$$\begin{cases} C_{sca} = \dfrac{W_{sca}}{I_{inc}}, \\ \\ C_{abs} = \dfrac{W_{abs}}{I_{inc}} = \dfrac{W_{ext} - W_{sca}}{I_{inc}}, \end{cases} \tag{1}$$

where I_{inc} is the incident irradiance, whereas W_{ext}, W_{sca}, and W_{abs} stand for the electromagnetic power extinguished, scattered, and absorbed by the particle, respectively. W_{sca} and W_{ext} are defined as the flux of the time-averaged Poynting vectors across an immaterial surface S around the particle:

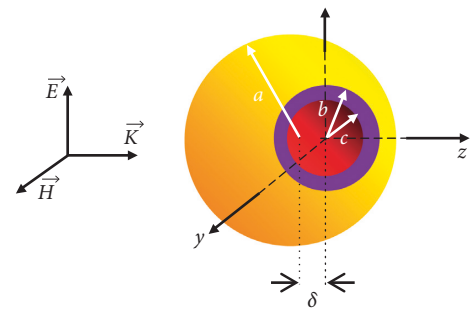

Figure 1: A schematic representation: a silicon/silica/gold spherical particle in space reported to the fixed coordinate system (O, x, y, and z) is illuminated by an x-polarized plane wave propagating along the z-axis. The centre of the silicon/silica nanoshell is taken as the origin of coordinates. a, b, and c are the radii of the silicon sphere, the silica shell, and the gold shell, respectively. δ measures the offset between the centre of the gold shell and the centre of the silicon/silica nanoshell.

$$\begin{cases} W_{sca} = \oint_S \langle \vec{E}_{sca} \wedge \vec{H}_{sca} \rangle \cdot \vec{n}\, ds, \\ W_{ext} = -\oint_S < \vec{E}_{inc} \wedge \vec{H}_{sca} + \vec{E}_{sca} \wedge \vec{H}_{inc} > \cdot \vec{n}\, ds, \end{cases} \tag{2}$$

where $(\vec{E}_{inc}, \vec{H}_{inc})$ and $(\vec{E}_{sca}, \vec{H}_{sca})$ are the incident and the scattered electromagnetic fields, respectively.

For a particle of simple geometrical form, one introduces dimensionless cross sections called the scattering efficiency Q_{sca} and absorption efficiency Q_{abs}; they are defined by the following equation:

$$\begin{cases} Q_{sca} = \dfrac{C_{sca}}{G}, \\ \\ Q_{abs} = \dfrac{C_{abs}}{G}, \end{cases} \tag{3}$$

where G is the particle cross-sectional area projected onto a plane perpendicular to the incident beam (for a spherical particle, $G = \pi a^2$).

An exact solution of Maxwell's equations can be accomplished analytically using the Lorenz–Mie theory [28]. This theory, however, is restricted to cases of centrosymmetric spheres and axiosymmetric cylinders. For the other cases, we are satisfied with an approximate resolution. The finite-difference time-domain (FDTD) method or Yee's method [29, 30] is proved to be a numerical analysis technique of choice. A detailed description of the FDTD method can be reviewed elsewhere (for example, refer [31]). In our present work, we have used commercialized FDTD Lumerical software.

3. Results and Discussion

The formalism described above is used to compute optical response of a single Si/SiO_2/Au multishell spherical nanoparticle immersed in a biological tissue of refractive index 1.44 [21]. Values of the complex indexes of refraction measured for bulk amorphous SiO_2 [32], bulk crystalline

silicon [33], and bulk crystalline gold [34] were used. The missing data were interpolated from the available experimental data by the cubic spline interpolation method. For gold, the complex refractive index was corrected for the nanoparticle size [35]. The refractive indexes n and the extinction coefficients κ for the three materials considered here are shown as curves in Figure 2 over the wavelength range 200–1500 nm.

3.1. Si/Au Concentric Nanoshell. Before approaching the Si/SiO_2/Au multishell nanoparticle, which is the main objective of this study, we decided to return to the ideal case of a Si/Au concentric nanoshell. As mentioned above, the latter has already been the subject of our previous work, but the host matrix was air. This time the medium in which the nanoshell is immersed is a biological tissue. The scattering and absorption efficiencies of such nanostructure are plotted in two-dimensional colour maps as a function of the particle diameter $D(=2a)$ and the wavelength in vacuum λ; the results are shown in Figure 3. Our calculations are given for particle diameters in the $10-500$ nm range, a fixed shell thickness fraction $t_f(=(b-a)/b)$ of 0.28, and for wavelengths in the $200-1400$ nm range.

An overall observation of these colour maps shows the same overall aspect as that obtained for a Si/Au nanoshell in air [26]. In particular, for $t_f < 0.5$, an intense branch of absorption resonances is distinguished above $\lambda = 600$ nm, attributed to the so-called surface plasmon resonances. It manifests itself for particle diameters in the range $\sim 50-150$ nm, irrespective of the shell thickness fraction, and over a corresponding finite spectral range, which redshifts by reducing the gold shell thickness fraction. The spectral range of this absorption branch lies well within the NIR window of the biological tissue [36] that is identified on the maps of Figure 3 by vertical dashed lines. For $t_f = 0.28$, for example, incident radiations of wavelengths close to 870 nm are absorbed efficiently by Si/Au nanoshells with diameters close to 95 nm. On the contrary, the scattering efficiency colour maps displayed in the bottom of Figure 3 highlight a relatively low scattering efficiency corresponding to the SPR branch. Thus, the Si/Au nanoparticles of sizes close to 95 nm in biological tissues absorb almost totally the light in the first spectral window. Larger nanoparticles, by cons, scatter completely the incident light in the second window. These observations are made more evident in Figure 4 by showing a direct comparison between the curves of absorption and scattering efficiencies of light by a Si/Au nanoshell in human tissues with an outer diameters of 95 nm and 220 nm and a shell thickness fraction of 0.28. Figure 4 also shows a similar comparison between the curves of absorption and scattering efficiencies of light by the Si/Au nanoshell in vacuum with a thickness fraction of 0.28 and outer diameters of 140 and 250 nm corresponding to the maximum absorption and the maximum scattering of light within the second window, respectively. A careful examination of Figure 4 shows a more efficient absorption of light in the first window by the Si/Au nanoparticles in the biological tissue and, in addition, with smaller sizes. Still interesting is the significant enhancement of the light scattering efficiency in the second spectral window when inserting the Si/Au particles into a biological tissue. As a matter of fact, resonances of absorption and scattering of light by Si/Au nanoshells in biological tissues are found to be more intense in efficiency than those supported by Si/Au nanoparticles in air.

In order to further characterize the optical properties of Si/Au nanoparticles in biological tissues interacting with incident light, we examined the distribution of the relative electric field intensity ($|E|^2/|E_{inc}|^2$) within and around the nanoparticle. Figure 5 shows colour maps of the relative electric field intensity in the main section xoz of the nanoparticle containing the incident polarization direction and the propagation direction. Those colour maps are drawn up for wavelengths corresponding to the maximum absorption resonance in the first window and the maximum scattering resonance in the second window. For comparison, Figure 5 also shows the maps corresponding to the Si/Au nanoparticle in air. To facilitate direct comparison between the two host media, we used the same colour scale. In biological tissues, the electric field intensity reaches much higher values than in the air. More interesting is that the biological tissue results in a more intense confinement of the electric field in the silicon core and therefore a more efficient absorption inside the nanoparticle. For infrared scattering resonance in the biological tissue, the electric field in the core becomes much less intense compared to what it was when the medium was the vacuum, which explains the dominance of the scattering on the absorption in the second spectral window when the host medium is the biological tissue.

The results obtained from this preliminary study carried out on silicon/gold core/shell nanoparticles in biological tissues highlight the fact that these nanostructures are potential candidates for bioimaging and photothermal therapy applications.

3.2. Si/SiO_2/Au Concentric Multishell. We now return to our main system, namely, the Si/SiO_2/Au multishell in biological tissues. We first start with the ideal case which consists of a concentric heterostructure, shown schematically at the top of Figure 6. Figure 6 displays a direct comparison between the absorption efficiency curves, on the one hand, and between the corresponding scattering efficiency curves, on the other hand, for two Si/SiO_2/Au multishells with total diameters of 95 nm and 220 nm, a gold shell thickness fixed at 13.3 nm and 30.8 nm, respectively, but a silica shell of variable thickness. Note that, in the absence of the silica shell, we find the concentric Si/Au nanoshells with diameters of 95 nm and 220 nm and a gold shell thickness fraction of 0.28, which have already been the subject of the previous section. For the comparison, the corresponding absorption and scattering curves are shown in the same figure with black lines.

From Figure 6, it is noted that the growth of the silica layer on the surface of the silicon core, while the gold shell thickness is kept fixed, which results in a blueshift of the absorption and scattering resonances supported by the original Si/Au nanoshell. This blueshift is found to be dependent

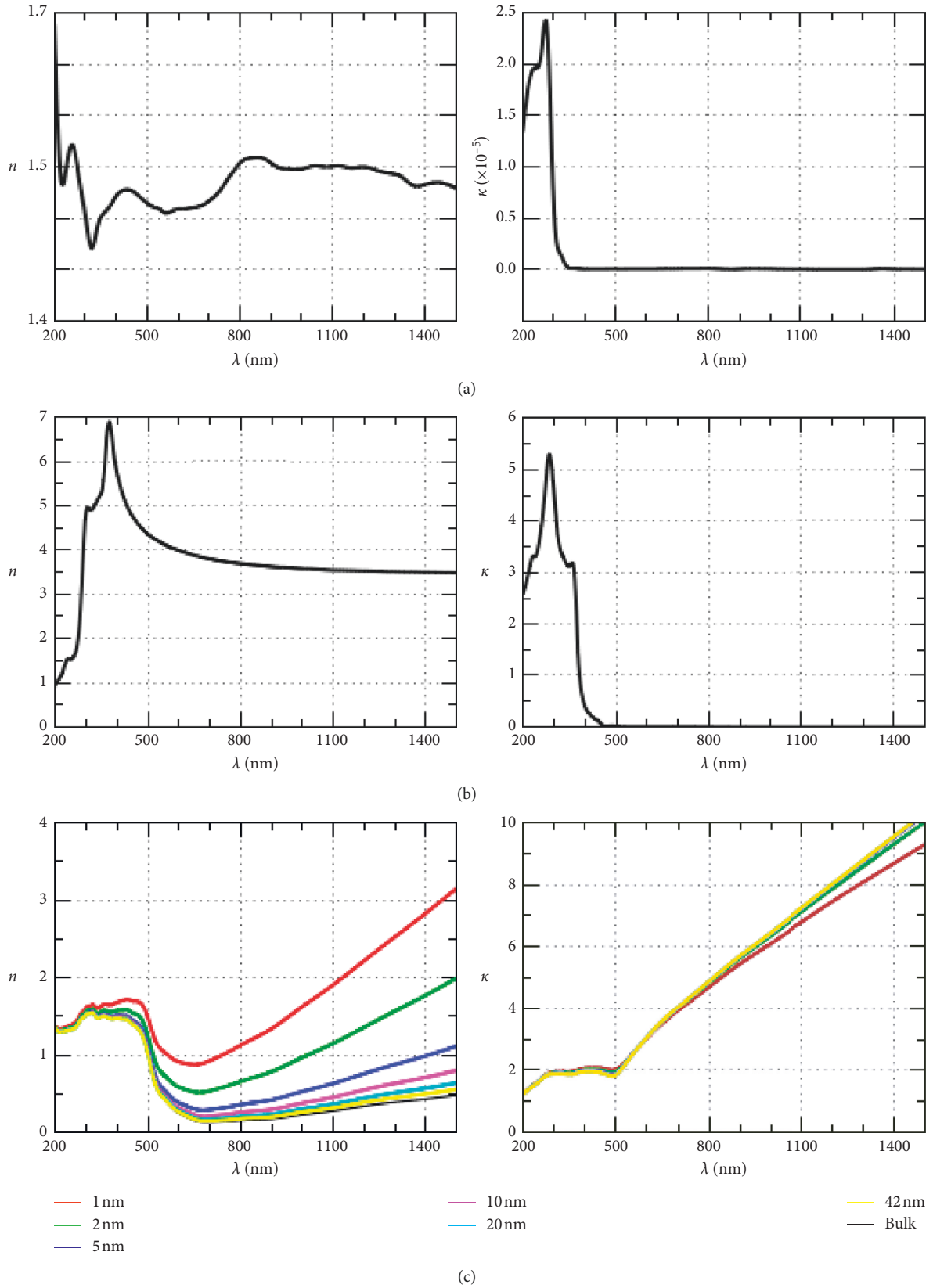

Figure 2: The refractive index n and the extinction coefficient κ of bulk silica (a), bulk silicon (b), and gold nanoparticles (c).

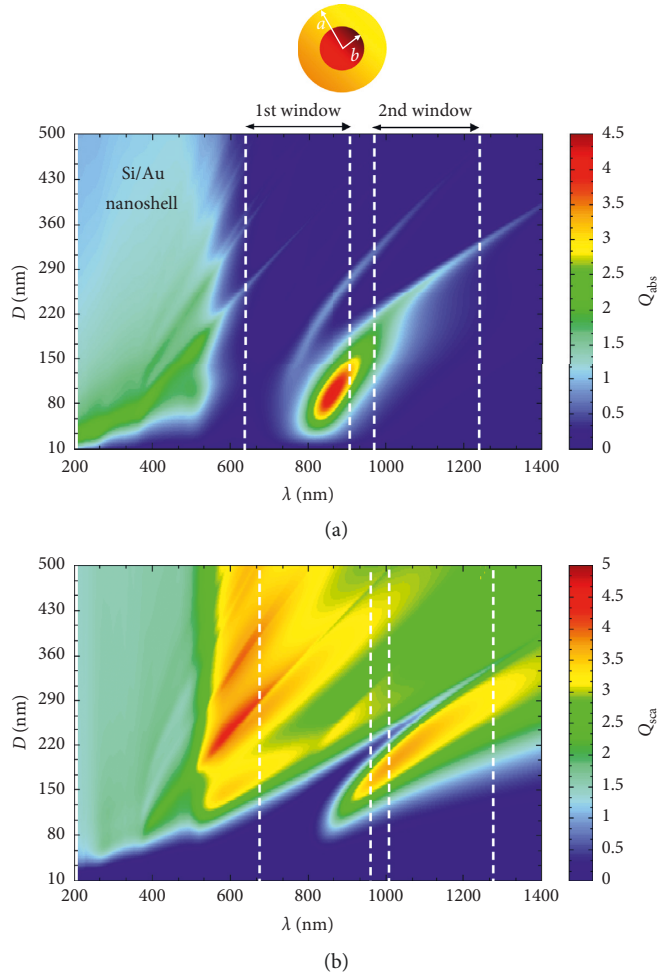

FIGURE 3: The absorption efficiency Q_{abs} (a) and scattering efficiency Q_{sca} (b) of a single Si/Au nanoshell in biological tissues as a function of the diameter D and the incident light wavelength λ. The vertical dashed lines delimit the optical windows of biological tissues.

on the silica layer thickness; indeed, it increases with the increasing thickness of the silica shell. For the thickness fraction of the gold shell and the thicknesses of the silica layer envisaged here, the most efficient absorption resonances still reside in the first spectral window of the biological tissue with the same, or even slightly better, magnitude as in the case without the silica shell. More quantitatively, the absorption band which was at 860 nm in the absence of silica is offset towards the lower limit of the first window, that is to say 700 nm, for a silica shell thickness of 6 nm. However, the corresponding scattering bands, which also lie within the first spectral window, gain importance with respect to the associated absorption bands; more quantitatively, the maximum relative efficiency of the scattering band increases from 27% in the absence of silica to 73% in the presence of a silica layer of 6 nm thick. On the contrary, the light scattering in the second spectral window of the biological tissue is still supported by the large $Si/SiO_2/Au$ multishell and, most interestingly, with the same efficiency as the case of the Si/Au parent nanoshell. Even more interesting is the fact that the corresponding absorption efficiency is weakened in the presence of the silica layer on the surface of the silicon core.

The distribution of the relative electric field intensity ($|E|^2/|E_{inc}|^2$) in the main section *xoz* of the $Si/SiO_2/Au$ concentric multishell interacting with a plane light wave is shown at the top of Figure 7 as two-dimensional colour maps. Those maps are established for two resonances observed on the curves of absorption and scattering efficiencies displayed in Figure 6 with the green colour: one at 726 nm corresponding to the absorption resonance and the other at 986 nm corresponding to the scattering resonance. As can be seen from the colour scale bar, the intensity of the electric field in the $Si/SiO_2/Au$ concentric multishell at the absorption resonance reaches values much greater than those supported by the parent Si/Au nanoshell of the same size and the same gold shell thickness; at the infrared scattering resonance, however, the maximum values of the intensity of the electric field are practically the same. Inside the multishell, the electric field is virtually entirely confined in the silica layer for both types of resonances.

3.3. $Si/SiO_2/Au$ Eccentric Multishell. After analyzing the effect of the silica layer between the silicon core and the gold shell on the response of a Si/Au concentric nanoshell in interaction with an electromagnetic plane wave, we now examine the effect of an eventual offset between the centre of

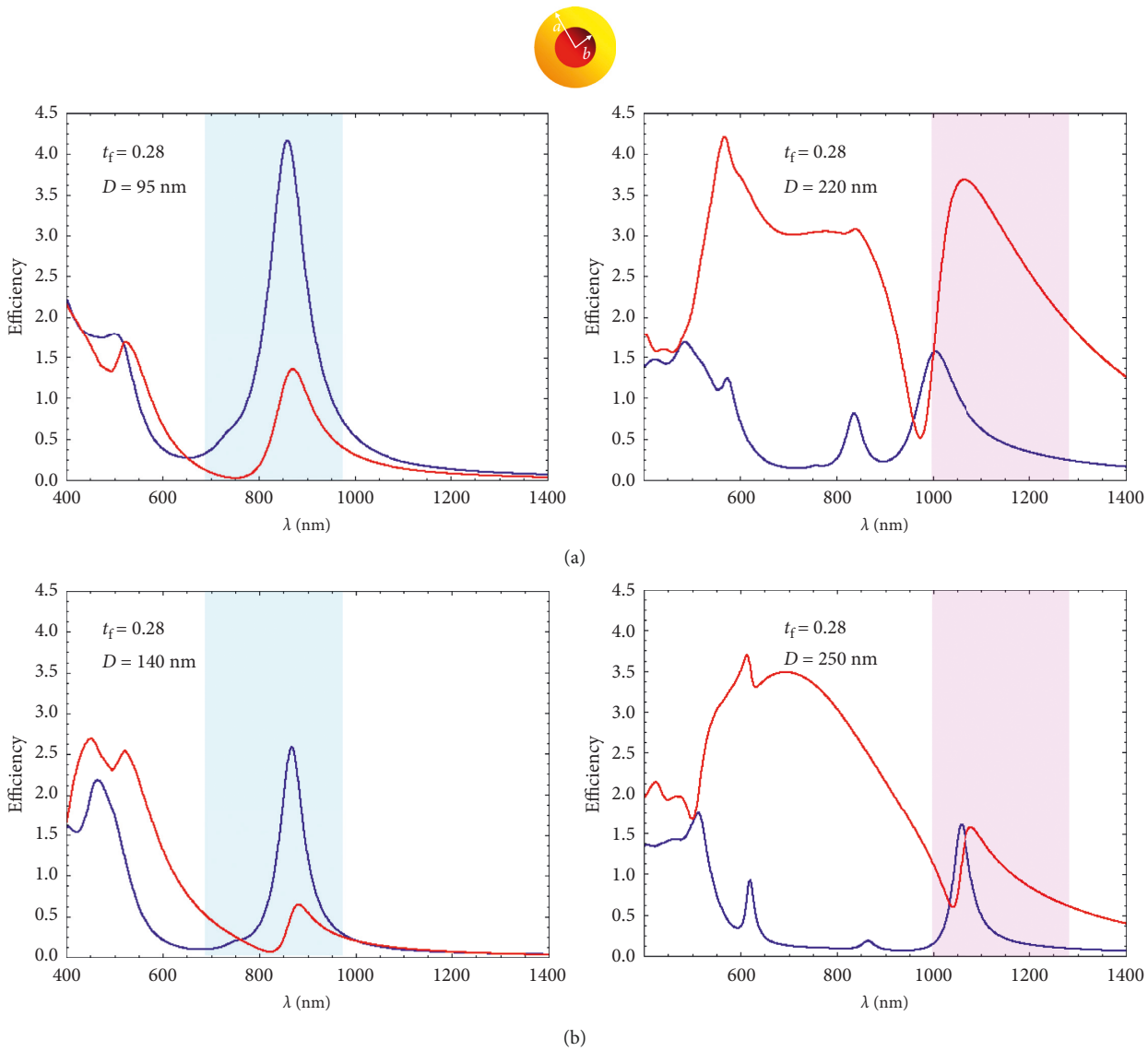

FIGURE 4: The absorption efficiency Q_{abs} (blue line) and scattering efficiency Q_{sca} (red line) of a single Si/Au nanoshell in biological tissues (a) and in vacuum (b) as a function of the incident light wavelength λ for selected nanoparticle diameters and a shell thickness fraction $t_f = 0.28$.

the Si/SiO_2 nanoshell and the centre of the gold shell. Hereinafter, this offset is denoted by δ, as indicated in the schematic representation of the eccentric $Si/SiO_2/Au$ multishell shown at the header of Figure 8. On the other contrary, we have limited ourselves to two configurations: one corresponding to an offset parallel to the direction of the electric field, that is to say parallel to the x-axis, and the other corresponding to an offset parallel to the magnetic field, that is to say parallel to the y-axis, with reference to Figure 1.

Recall that the problem of the eccentric $Si/SiO_2/Au$ multishell was recently undertaken by Wang et al. [37]. These authors considered the case where the silicon core is offset from the centre of the gold shell so that the latter holds its spherical symmetry and therefore a uniform thickness, while the silica layer is nonuniform around the silicon core. This case is obviously different from ours. In order to ensure that our software works well, we have reconsidered two of their nanostructures in vacuum, one concentric and the other eccentric with an offset of 15 nm in the direction of the incident electric field, and we have computed their scattering spectra. We have found practically the same results as obtained by these authors.

Our designed eccentric multishells are obtained by moving away the Si/SiO_2 nanoshell with respect to the centre of the gold shell; the gold shell thickness is therefore nonuniform around the Si/SiO_2 nanoshell. We have thus generated two sets of eccentric multishells: the first corresponds to an offset in the direction of the incident electric field by a distance δ_x, and the second corresponds to an offset in the direction of the incident magnetic field by a distance δ_y, in accordance with our choice of the axes system depicted in Figure 1. Two parent concentric $Si/SiO_2/Au$ multishells were

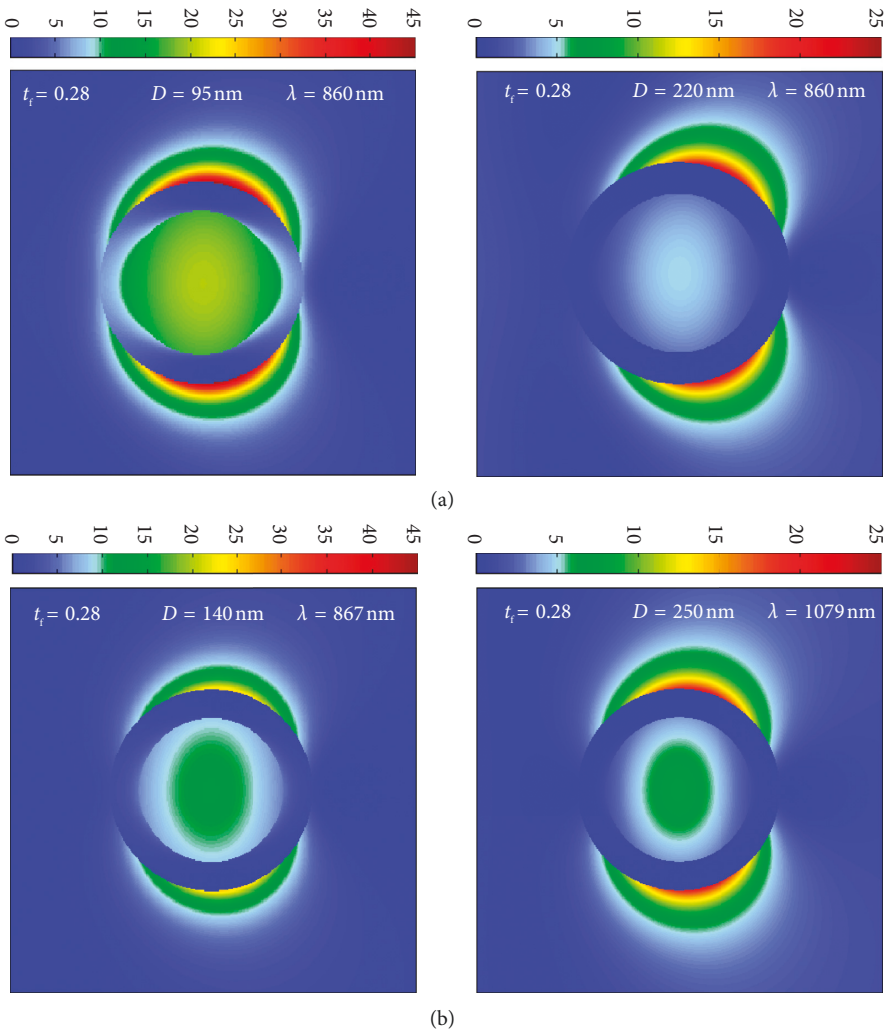

FIGURE 5: The spatial distribution in the *xoz* plane of the relative intensity of the electric field ($|E|^2/|E_{inc}|^2$) computed at selected wavelengths corresponding to relevant absorption and scattering resonances supported by a single Si/Au nanoshell in biological tissues (a) and in vacuum (b).

chosen among those studied in the previous section: one designated as 56/68/95 and the other as 146.4/158.4/220; both have a silica layer of 6 nm thick. The absorption efficiency curves calculated for the eccentric multishells derived from the first parent multishell are plotted in Figure 8; it also shows the scattering efficiency curves computed for the eccentric multishells derived from the second parent multishell. For comparison, we have displayed the curves corresponding to the parent concentric multishells in black colour.

An overall observation of Figure 8 shows that, for the values of the offsets considered here, the overall aspect of the absorption curves and that of the scattering curves of light by eccentric multishells is practically identical to those obtained with the parent concentric nanoparticles. A detailed observation shows, however, a redshift of the main resonance bands accompanied by a decrease in their amplitudes. On the contrary, a feature on the small wavelength side, which appears as a shoulder on the main absorption resonance band, grows and redshifts by increasing the nanoshell offset. Interestingly, when comparing Figure 8 with Figure 6, it can be seen that the effect of the growth of a silica layer on the silicon core, on the one hand, and the effect of the Si/SiO_2 offset with respect to the Au shell, on the other hand, are antagonistic. Indeed, the first causes the main resonance bands to move away from the spectral window of the biological tissue, whereas the second one brings them back into it. A close examination of Figure 8 also shows that the scattering efficiency is practically independent on the orientation of the offset direction relative to the polarization of the incident light. This is also the case for the absorption efficiency but with respect to the spectral positions of the resonance bands only; however, their intensities are offset direction dependent. The independence of the plasmon energies on the relative orientation of the gold shell offset is previously predicted by the plasmon hybridization theory developed by Wu and Nordlander [38] in gold nanoshells with a nonconcentric cavity.

The spatial distribution of the relative electric field intensity ($|E|^2/|E_{inc}|^2$) in a main section of the $Si/SiO_2/Au$ eccentric multishell interacting with an electromagnetic

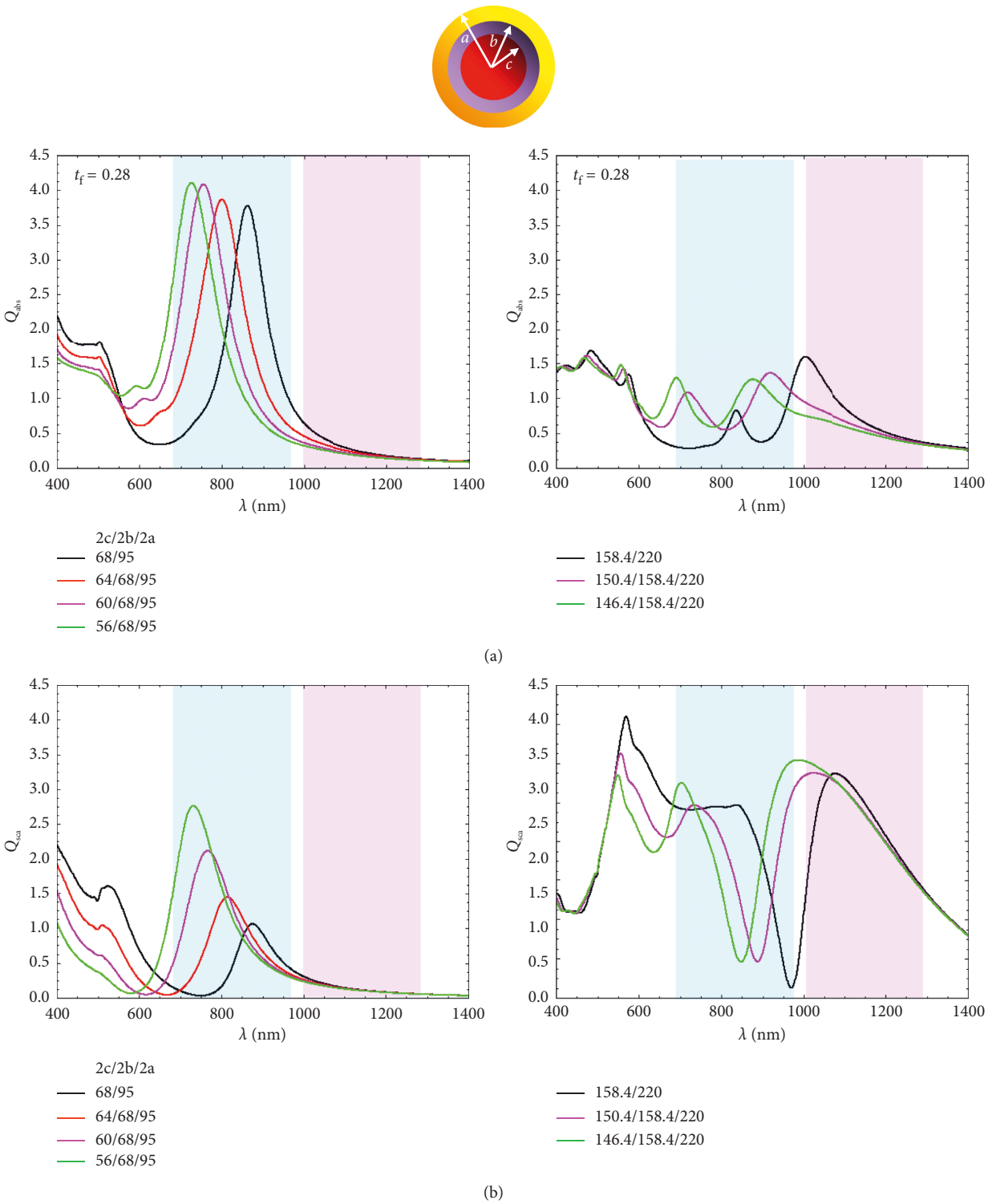

FIGURE 6: The absorption efficiency Q_{abs} (a) and scattering efficiency Q_{sca} (b) of a single $Si/SiO_2/Au$ concentric multishell in biological tissues as a function of the incident light wavelength λ for different silica shell thicknesses but fixed particle diameter and fixed gold shell thickness.

plane wave was computed numerically using the FDTD method. Two examples are shown as two-dimensional colour maps in the panels at the bottom of Figure 7; they correspond to the two multishells: 56/68/95 with an 11 nm offset and 146.4/158.4/220 with an 20 nm offset in the incident electric field direction. Those maps are established for two main resonances observed on the curves of absorption and scattering efficiencies displayed in Figure 8 in gray and green colours, respectively. Recall that the maps corresponding to the parent concentric multishells are also

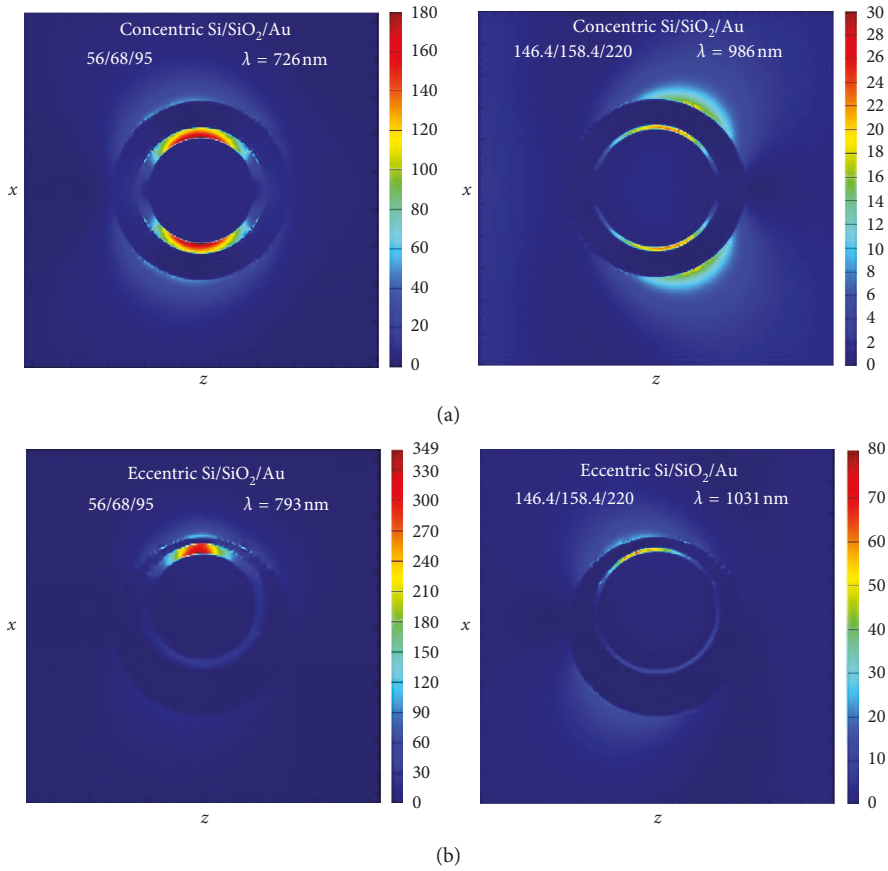

FIGURE 7: The spatial distribution in the *xoz* plane of the relative intensity of the electric field ($|E|^2/|E_{inc}|^2$) computed at selected wavelengths corresponding to relevant absorption and scattering resonances supported by a concentric (a) and eccentric (b) $Si/SiO_2/Au$ multishell in biological tissues.

shown in Figure 7 (the upper panels). As can be seen from the colour scale bars, the maximum of the electric field enhancement factor supported by the eccentric $Si/SiO_2/Au$ multishell far exceeds its counterpart in the parent concentric multishell, and this is true both at the absorption resonance and scattering resonance. In both cases, the maximum enhancement lies in the silica layer, as was the case in concentric multishells, but this time localized near the thin gold shell zone, forming the so-called hotspots. More interesting is the enhancement of the electric field at the nanoparticle-biological tissue interface. It is less important than that observed in the silica layer, but it is much more significant than its counterpart supported by the parent concentric multishell.

4. Conclusions

The present work is devoted to the simulation of the absorption and scattering efficiencies of light by a single $Si/SiO_2/Au$ spherical multishell embedded in a biological tissue. We first revised the ideal case of a concentric Si/Au nanoshell, analyzed the effect of growing a silica layer of uniform thickness around the silicon core concentric to the gold shell, and then examined the effect of centrosymmetry breakdown caused by an offset of the gold shell with respect to the centre of the Si/SiO_2 nanoshell. Our simulation showed that the Si/Au nanoparticle in the biological tissue supports absorption and scattering resonances within the biological optical window more significant than in vacuum. On the contrary, the growth of a uniform layer of silica on the surface of the silicon core leads to a blueshift of these resonances that increases with the thickness of this layer without significantly modifying their magnitudes. For low values of the silica layer thickness, no more than 6 nm, these absorption and scattering resonances still reside in the first- and second-optical windows of the biological tissue, respectively. The offset of the gold shell with respect to the Si/SiO_2 core results in a redshift of the absorption and scattering resonances supported by the concentric $Si/SiO_2/Au$ multishell within the biological window, accompanied by a decrease in their amplitudes. The magnitude of these effects depends, in fact, on the offset value and also on the direction of the offset with respect to the polarization of the incident light. Our findings thus show that the deviation from an Si/Au ideal nanostructure due to the growth of a silica layer at the silicon surface and/or a gold shell offset in no way diminishes the quality of its optical response. More interesting is a more prominent electric field enhancement at the eccentric multishell-biological tissue interface. These observations still make $Si/SiO_2/Au$

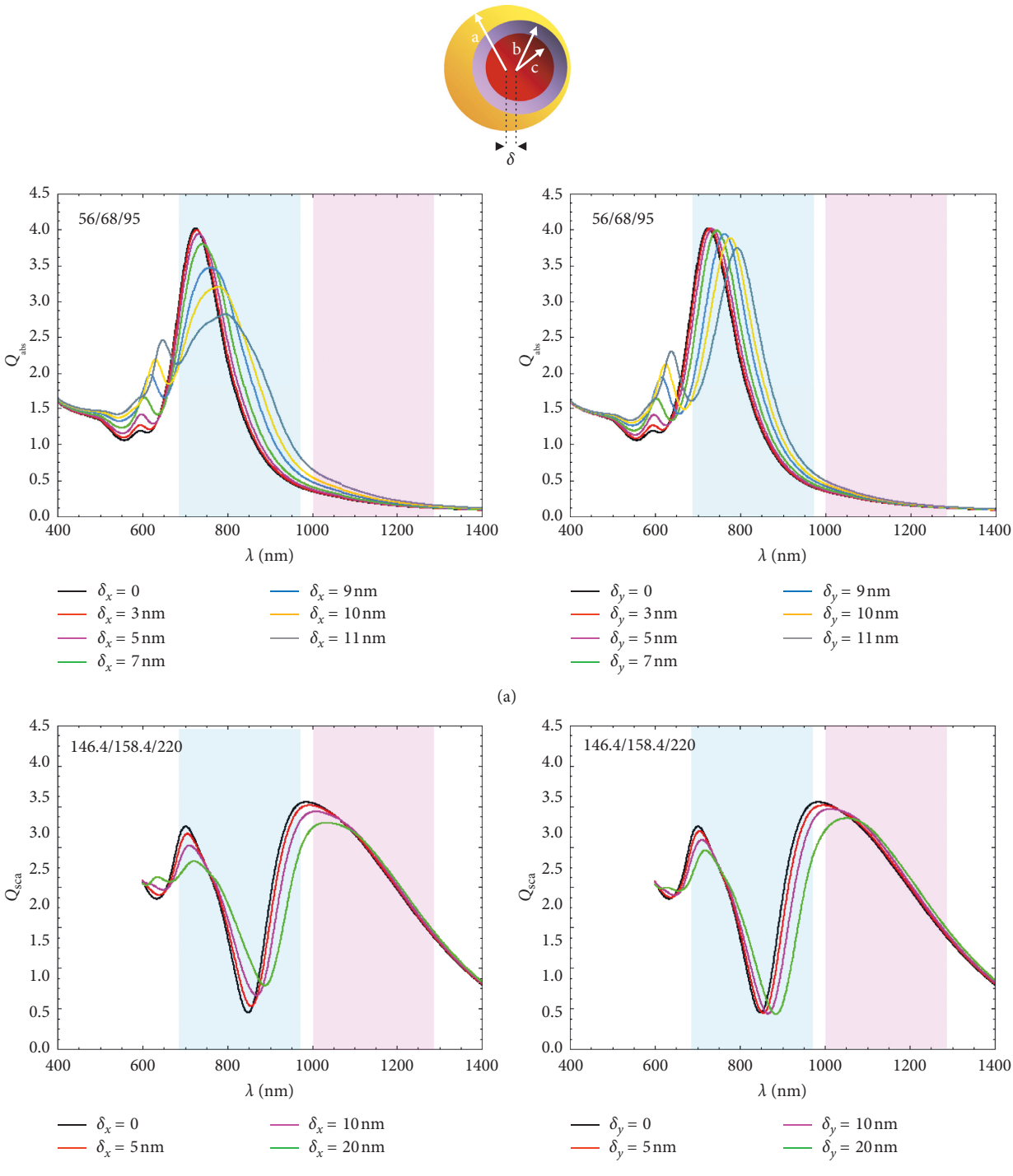

FIGURE 8: The absorption efficiency Q_{abs} (a) and scattering efficiency Q_{sca} (b) of a single $Si/SiO_2/Au$ eccentric multishell in biological tissues as a function of the incident light wavelength λ for different values of the gold shell offset.

multishells of potential candidates for bioimaging and photothermal therapeutic applications. The realization of these observations on the practical level is our challenge at the moment.

Data Availability

The data used to support the findings of this study are available from the corresponding author upon request.

Disclosure

The results of the present work have been presented in the International Nanotech and NanoScience Conference and Exhibition Nanotech France 2017 held in Paris from 28 to 30 June 2017.

Conflicts of Interest

The authors declare that there are no conflicts of interest regarding the publication of this paper.

References

[1] A. Otto, "Excitation of nonradiative surface plasma waves in silver by the method of frustrated total reflection," *Zeitschrift für Physik A Hadrons and nuclei*, vol. 216, no. 4, pp. 398–410, 1968.

[2] C. Loo, A. Lin, L. Hirsch et al., "Nanoshell-enabled photonics-based imaging and therapy of cancer," *Technology in Cancer Research and Treatment*, vol. 3, no. 1, pp. 33–40, 2016.

[3] M. Bikram, A. M. Gobin, R. E. Whitmire, and J. L. West, "Temperature-sensitive hydrogels with SiO2-Au nanoshells for controlled drug delivery," *Journal of Controlled Release*, vol. 123, no. 3, pp. 219–227, 2007.

[4] Y. Cheng, G. Lu, H. shen et al., "Highly enhanced spontaneous emission with nanoshell-based metallodielectric hybrid antennas," *Optics Communications*, vol. 350, pp. 40–46, 2015.

[5] A. Saini, T. Maurer, I. I. Lorenzo et al., "Synthesis and SERS application of SiO2@Au nanoparticles," *Plasmonics*, vol. 10, no. 4, pp. 791–796, 2014.

[6] A. M. Gobin, M. H. Lee, N. J. Halas, W. D. James, R. A. Drezek, and J. L. West, "Near-infrared resonant nanoshells for combined optical imaging and photothermal cancer therapy," *Nano Letters*, vol. 7, no. 7, pp. 1929–1934, 2007.

[7] T. A. Erickson and J. W. Tunnell, "Gold nanoshells in biomedical applications," in *Nanomaterials for the Life Sciences: Mixed Metal Nanomaterials*, pp. 1–44, vol. 3, pp. 1–44, Wiley-VCHGmbH Verlag and Co, Weinheim, Germany, 2009.

[8] D. P. Modi, S. Chaudhary, R. Shah, and D. J. Sen, "Gold nanoshell: the advancing nanotechnology to fight against cancer," *British Biomedical Bulletin*, vol. 1, pp. 23–34, 2013.

[9] J. Zhao, M. Wallace, and M. P. Melancon, "Cancer theranostics with gold nanoshells," *Nanomedicine*, vol. 9, no. 13, pp. 2041–2057, 2014.

[10] R. Huschka, J. Zuloaga, M. W. Knight, L. V. Brown, P. Nordlander, and N. J. Halas, "Light-induced release of DNA from gold nanoparticles: nanoshells and Nanorods," *Journal of the American Chemical Society*, vol. 133, no. 31, pp. 12247–12255, 2011.

[11] W. Zheng, H. C. Chiamori, G. L. Liu, L. Lin, and F. F. Chen, "Nanofabricated plasmonic nano-bio hybrid structures in biomedical detection," *Nanotechnology Reviews*, vol. 1, no. 3, pp. 213–233, 2012.

[12] J. A. Gordon and R. W. Ziolkowski, "The design and simulated performance of a coated nano-particle laser," *Optics Express*, vol. 15, no. 5, pp. 2622–2653, 2007.

[13] K. Tanabe, "Field enhancement around metal nanoparticles and nanoshells: a systematic investigation," *The Journal of Physical Chemistry C*, vol. 112, no. 40, pp. 15721–15728, 2008.

[14] O. Peña, U. Pal, L. Rodríguez-Fernández, and A. Crespo-Sosa, "Linear optical response of metallic nanoshells in different dielectric media," *Journal of the Optical Society of America B*, vol. 25, no. 8, pp. 1371–1379, 2008.

[15] R. Bardhan, N. K. Grady, T. Ali, and N. J. Halas, "Metallic nanoshells with semiconductor cores: optical characteristics modified by core medium properties," *ACS Nano*, vol. 4, no. 10, pp. 6169–6179, 2010.

[16] A. E. Miroshnichenko, "Off-resonance field enhancement by spherical nanoshells," *Physical Review A*, vol. 81, no. 5, pp. 053818–053822, 2010.

[17] X. Zhou, H. Li, S. Xie, S. Fu, H. Xu, and Z. Liu, "Effects of dielectric core and embedding medium on plasmonic coupling of gold nanoshell arrays," *Solid State Communications*, vol. 151, no. 14-15, pp. 1049–1052, 2011.

[18] P. Tuersun, X. e. Han, and K. F. Ren, "Backscattering properties of gold nanoshells: quantitative analysis and optimization for biological imaging," *Procedia Engineering*, vol. 102, pp. 1511–1519, 2015.

[19] N. Hooshmand, P. K. Jain, and M. A. El-Sayed, "Plasmonic spheroidal metal nanoshells showing larger tunability and stronger near fields than their spherical counterparts: an effect of enhanced plasmon coupling," *Journal of Physical Chemistry Letters*, vol. 2, no. 5, pp. 374–378, 2011.

[20] H. Suzuki and I.-Y. Sandy Lee, "Mie scattering field inside and near a coated sphere: computation and biomedical applications," *Journal of Quantitative Spectroscopy and Radiative Transfer*, vol. 126, pp. 56–60, 2013.

[21] D. Sikdar, I. D. Rukhlenko, W. Cheng, and M. Premaratne, "Effect of number density on optimal design of gold nanoshells for plasmonic photothermal therapy," *Biomedical Optics Express*, vol. 4, no. 1, pp. 15–31, 2012.

[22] A. SalmanOgli and A. Rostami, "Investigation of surface plasmon resonance in multilayered onion-like hetero-nanocrystal structures," *IEEE Transactions on Nanotechnology*, vol. 12, no. 5, pp. 831–838, 2013.

[23] Y. Huang and L. Gao, "Superscattering of light from core-shell nonlocal plasmonic nanoparticles," *Journal of Physical Chemistry C*, vol. 118, no. 51, pp. 30170–30178, 2014.

[24] K. Laaksonen, S. Suomela, S. R. Puisto, N. K. J. Rostedt, T. Ala-Nissila, and R. M. Nieminen, "Influence of high-refractive-index oxide cores on optical properties of metal nanoshells," *Journal of the Optical Society of America B*, vol. 31, no. 3, pp. 494–502, 2014.

[25] J. Sancho-Parramon and D. Jelovina, "Boosting Fano resonances in single layered concentric core-shell particles," *Nanoscale*, vol. 6, no. 22, pp. 13555–13564, 2014.

[26] W. Chaabani, A. Chehaidar, and J. Plain, "Comparative theoretical study of the optical properties of silicon/gold, silica/gold core/shell and gold spherical nanoparticles," *Plasmonics*, vol. 11, no. 6, pp. 1525–1535, 2016.

[27] W. Wu, M. Wan, P. Gu, Z. Chen, and Z. Wang, "Strong coupling between few molecular excitons and Fano-like cavity plasmon in two-layered dielectric-metal core-shell resonators," *Optics Express*, vol. 25, no. 2, pp. 1495–1509, 2017.

[28] C. F. Bohren and D. R. Huffman, *Absorption and Scattering of Light by Small Particles*, John Wiley & Sons, New York, NY, USA, 1998.

[29] K. S. Yee, "Numerical solution of initial boundary value problems involving Maxwell's equations in isotropic media," *IEEE Transactions on Antennas and Propagation*, vol. 14, no. 3, pp. 302–307, 1966.

[30] A. Taflove, "Application of the finite-difference time-domain method to sinusoidal steady-state electromagnetic-penetration problems," *IEEE Transactions on Electromagnetic Compatibility EMC*, vol. 22, no. 3, pp. 191–202, 1980.

[31] U. S. Inan and R. A. Marshall, *Numerical Electromagnetics, the FDTD method*, Cambridge University Press, Cambridge, UK, 2011.

[32] M. A. Khashan and A. Y. Nassif, "Dispersion of the optical constants of quartz and polymethyl methacrylate glasses in a wide spectral range: 0.2-3μm," *Optics Communications*, vol. 188, no. 1–4, pp. 129–139, 2001.

[33] J. Humlícek, "Properties of silicon, germanium and SiGe: carbon," in *EMIS Datareviews Series*, E. Kasper and K. Lyutovich, Eds., Vol. 24, INSPEC, London, UK, 2000.

[34] P. B. Johnson and R. W. Christy, "Optical constants of the noble metals," *Physical Review B*, vol. 6, no. 12, pp. 4370–4379, 1972.

[35] G. Raschke, S. Brogl, A. S. Susha et al., "Gold nanoshells improve single nanoparticle molecular sensors," *Nano Letters*, vol. 4, no. 10, pp. 1853–1857, 2004.

[36] A. M. Smith, M. C. Mancini, and S. Nie, "Second window for in vivo imaging," *Nature Nanotechnology*, vol. 4, no. 11, pp. 710-711, 2009.

[37] W. Wang, Y. Wang, Y. Shi, and Y. Liu, "Magnetic-Based double fano resonances in Au-SiO2-Si multilayer nanoshells," *Plasmonics*, vol. 12, no. 5, pp. 1537–1543, 2016.

[38] Y. Wu and P. Nordlander, "Plasmon hybridization in nanoshells with a nonconcentric core," *Journal of Chemical Physics*, vol. 125, no. 12, pp. 124708–124717, 2006.